Interplay between Coulomb interaction and quantum interference in three-level resonant asymmetric double quantum wells

P. M. Alsing,[1,2,3] D. H. Huang,[1] D. A. Cardimona,[1] and T. Apostolova[1]
[1]*Air Force Research Lab (AFRL/VSSS), Kirtland Air Force Base, New Mexico 87117, USA*
[2]*The Albuquerque High Performance Computing Center and The Center for Advanced Studies, University of New Mexico, Albuquerque, New Mexico 87131, USA*
[3]*Department of Physics and Astronomy, University of New Mexico, Albuquerque, New Mexico 87131, USA*
(Received 11 March 2003; published 12 September 2003)

A many-body density-matrix theory is derived by including quasiparticle renormalization of kinetic energy and dipole coupling to an external electromagnetic field, as well as the screening and quantum-interference effects. This theory is applied to a three-level resonant asymmetric double-quantum-well system in which the ground subband is coupled to the upper tunneling-split doublet by a strong external electromagnetic field. By using this theory, the quasiparticle energy-level separations and off-diagonal radiative-decay coupling rates, absorption coefficient, refractive-index function, and scaled subband electron density are calculated as functions of incident photon energy. The effects of quasiparticle renormalization on the quantum interference between a pair of optically induced polarizations are analyzed. The quantum interference is shown to be robust against the Coulomb-interaction effect in the mean-field approximation. The roles played by the dephasing rate and electron density are explained.

DOI: 10.1103/PhysRevA.68.033804 PACS number(s): 42.50.Ct, 42.50.Hz, 42.50.Md

I. INTRODUCTION

When an electromagnetic field is applied to a resonant asymmetric double-quantum-well system, there exists *quantum interference* between a pair of optically induced polarizations of the system [1]. The quantum-interference effect is found to be a result of the off-diagonal radiative-decay coupling (ODRDC) [2,3] which can be systematically derived from a quantum electrodynamic treatment of photons and electrons in second quantization. The effect of ODRDC describes a nearly resonant absorption of a spontaneously emitted photon from one downward electron transition by another upward electron transition. In addition, the ODRDC effect in the bare-atom picture of a three-level atomic system is equivalent to the electromagnetically induced transparency effect [4] in the dressed-atom picture, and the effect of probe-field gain based on an ODRDC process is connected to an amplification without inversion [5] in the bare-atom picture of a three-level atomic system [6].

For noninteracting electrons in quantum wells, both absorption-peak position and strength are fully determined by the energy-level separation and wave functions derived from the Schrödinger equation. When the *Coulomb interaction* between electrons is taken into consideration, interacting electrons will form quasiparticles with renormalization of both kinetic energy and dipole coupling to an external electromagnetic field [7,8]. The kinetic-energy renormalization includes positive Hartree and negative Fock corrections. The former tends to push energy levels up, while the latter tends to drag energy levels down [8]. The renormalization of dipole coupling to an external field is caused by the optically-induced polarization of the system [7]. In addition to quasiparticle energy renormalization, optically excited electrons which will polarize the system by creating a statistical dipole moment try to screen the Coulomb interaction between electrons, leading to a depolarization shift of the absorption peak. [8] If we further look on a femtosecond-time scale, the quantum kinetics of electrons due to Coulomb scattering plays a major role in the absorption spectrum of electrons in quantum wells [7].

In order to fully incorporate the effects of the Coulomb interaction and quantum interference, we need to generalize the many-body density-matrix equations [7]. The conventional calculation for Coulomb-interaction effects is based on a perturbation to the system [8], where the electron distribution function is kept as the equilibrium Fermi-Dirac function. The existence of a quantum-interference effect introduces a nonequilibrium distribution of electrons and causes the distribution to depend on the frequency of an incident electromagnetic field. As a result, both the quasiparticle energy renormalization and many-body screening, which determine the peak position and strength, are altered by the incident photon energy. On the other hand, whenever there exists an absorption peak under a strong electromagnetic field, there will be a minimum in the density of electrons in the ground subband at that specific photon energy due to transferring electrons from the ground subband to higher subbands. Therefore, the ODRDC effect will also be modified by the photon energy through the Coulomb interaction between electrons since its coupling rate is proportional to the cube of the energy-level separation.

In this paper, we will address the following question. How do many-body effects alter the quantum interference seen in the single-particle absorption spectrum? We will first derive the many-body density-matrix equations by including quasiparticle renormalization of the kinetic energy and dipole coupling to an external electromagnetic field, as well as the screening and quantum-interference effects. We then apply our theory to a three-level resonant asymmetric double-quantum-well system in which the ground subband is coupled to the upper resonant doublet by a strong electro-

magnetic field. Finally, using this theory we calculate the renormalized energy-level separations, off-diagonal radiative-decay coupling rates, absorption coefficients, refractive-index functions, and scaled first-subband electron density as functions of incident photon energy. The Coulomb-interaction effect on the quantum interference is analyzed. The quantum-interference effect is found to be robust against the Coulomb interaction between electrons in the mean-field approximation. In addition, roles played by the dephasing rate and electron density are discussed.

The organization of this paper is as follows. Section II is devoted to the derivation of a many-body density-matrix theory for the calculation of time-resolved absorption spectra, including quantum-interference effects. Numerical results and discussions are presented in Sec. III for the optical spectra in three-level resonant asymmetric double quantum wells, where the quasiparticle energy-level renormalization, screening effect, and quantum-interference effect are analyzed and explained. The paper is briefly concluded in Sec. IV.

II. MODEL AND THEORY

In this paper, we only consider the dynamics of the radiative decay of conduction electrons in an intersubband-transition quantum-well system. The scattering effects (energy relaxation and dephasing of optical coherence) from other electrons, phonons, impurities, and interface roughness will be taken into account simply by introducing a homogeneous level broadening in steady state for electrons in quantum wells. The renormalization of kinetic energy and dipole coupling is included under the mean-field approximation. The screening effect is incorporated into our theory in the long-wavelength limit under the self-consistent-field approach. The quantum interference between optically induced polarizations is considered in a quantum electrodynamic treatment of spontaneous emission under the rotating-wave approximation.

Detailed discussions on including many-body effects in density-matrix equations can be found in a book edited by Chow and Koch [9]. In this section, we will first present a brief review of semiconductor quantum wells. After that, the importance of the Coulomb interaction between electrons will be discussed and a criteria for including the Coulomb interaction will be given. Finally, many-body density-matrix equations will be derived by including the quantum-interference effect on electron intersubband transitions in a three-level resonant asymmetric double-quantum-well system. Based on these equations, optical spectra will be calculated for different dephasing rates and electron densities, and effects of the Coulomb interaction on the quantum interference between optically induced polarizations will be analyzed.

A. Semiconductor quantum wells

Bulk III-V binary semiconducting compounds, such as InP, InAs, InSb, GaP, GaAs, GaSb, AlAs, AlSb, etc., crystallize in the zinc-blende structure [10]. Their lattices consist of two interpenetrating, face-centered cubic lattices, displaced from one another along one of their main diagonals by a distance equal to one-fourth of this diagonal. The top of the valence band occurs at the center of the Brillouin zone (Γ point). The conduction-band edge is found either at the Γ ([000]) point or near the L ([111]) or the X ([001]) point. The energy difference between the top of the valence band and the bottom of the conduction band is called the band gap E_G, which usually depends on the temperature. For ternary alloy materials, such as $Al_xGa_{1-x}As$, $In_xGa_{1-x}As$, $Al_xGa_{1-x}Sb$, etc., E_G also depends on the alloy composition index x.

When a binary compound, such as GaAs, is sandwiched between ternary alloy materials, such as $Al_xGa_{1-x}As$, or between different binary compounds, such as AlAs, the difference in their band gaps ΔE_G causes the bottom of the conduction band and the top of the valence band to take on a stepped shape in the resulting heterostructure. The step height in the conduction band is ΔE_c while the step height in the valence band is ΔE_v with $\Delta E_c + \Delta E_v = \Delta E_G$. The electrons in the GaAs ''well'' material become confined by the potential barrier ΔE_c. Similarly, the holes in the GaAs ''well'' material are also confined by the potential barrier ΔE_v. If the width of the GaAs layer is comparable to the de Broglie wavelengths of the electrons and holes, the whole system will enter into a quantum regime, with particle motion across the layers quantized [10]. In this case, we term this ''well'' a quantum well.

In this paper, we only discuss the intersubband transitions of conduction electrons in quantum wells. Noninteracting particles, such as electrons, inside a quantum well (confined in the z direction) obey the Schrödinger equation

$$-\frac{\hbar^2}{2}\frac{d}{dz}\left[\frac{1}{m^*(z)}\frac{d}{dz}\right]\phi(z)+U_{QW}(z)\phi(z)=E\phi(z), \quad (1)$$

where $m^*(z)$ is the effective mass m_W (m_B) of the electron in the well (barrier) material, E is the energy of the electron, $U_{QW}(z)=\Delta E_c$ is the height of the potential barrier of the quantum well for the electron, and $\phi(z)$ is the wave function of the electron in the quantum well. It is easy to show that the energy E of the electron in the quantum well will be quantized into multiple subbands $E_j^{(0)}(k)$ with level index $j=1, 2, 3, \ldots$, where k is the in-plane (perpendicular to the z direction) wave vector of the electron due to its free motion within the plane [10]. The corresponding wave function for each subband $E_j^{(0)}(k)$ is denoted by $\phi_j(z)$. The energy of the electron in the quantum well can be written as

$$E_j^{(0)}(k)=E_j+\frac{\hbar^2k^2}{2m_j^*(k)}, \quad (2)$$

which has a nonparabolic dispersion. Here E_j is the edge of the jth subband. A large nonparabolic effect can destroy the quantum interference in the system [1]. The effective k-dependent effective mass $m_j^*(k)$ of the electron in Eq. (2) is found to be [8]

$$\frac{1}{m_j^*(k)}=\frac{P_j}{m_j(k)}+\frac{1-P_j}{m_B}, \tag{3}$$

where P_j is the quantum-well dwelling probability for the electron in the jth subband and $m_j(k)$ is given by [8]

$$\frac{m_0}{m_j(k)}=1+\frac{E_p}{3}\left[\frac{2}{E_G+E_j+\hbar^2k^2/2m_W}+\frac{1}{E_G+\Delta_0+E_j+\hbar^2k^2/2m_W}\right] \tag{4}$$

with free-electron mass m_0. In Eq. (4), E_G and Δ_0 are the energy gap and spin-orbit splitting for the well material, respectively, and E_p is the interband Kane matrix element [1]. The complete form of the wave function for a single electron in the quantum well can be written as

$$\psi_{j\vec{k}}(\vec{r})=\frac{1}{\sqrt{2\pi}}\exp(\vec{k}\cdot\vec{r}_\parallel)\phi_j(z), \tag{5}$$

where $\vec{r}=(\vec{r}_\parallel,z)$ with $\vec{r}_\parallel$ being a two-dimensional position vector in the plane perpendicular to the growth direction, and the plane-wave part of the wave function corresponds to the free (nonquantized) motion experienced by the electron within this plane. For simplicity, we only show here the envelope part of the wave function [1] for the electron in the quantum well. The Bloch function associated with the wave function in the bulk material and the spinor part of the wave function for electron spins are irrelevant for discussing the intersubband transitions of conduction electrons.

B. Importance of Coulomb interaction

Let us start by considering a single quantum well which contains an electron gas. At zero temperature ($T=0$ K), the maximum kinetic energy of a noninteracting-electron gas is the Fermi energy, defined by

$$E_F=\frac{\hbar^2k_F^2}{2m_W}, \tag{6}$$

where $k_F=\sqrt{2\pi n_{2D}}$ is the Fermi wave vector and n_{2D} is the two-dimensional density of electrons in the quantum well. If we define the mean distance $\overline{R}$ between two electrons by

$$\frac{4}{3}\pi\overline{R}^3n_{3D}=1, \tag{7}$$

where $n_{3D}=n_{2D}/L_W$ and L_W is the width of the quantum well, the average excitonic interaction between two electrons is [6]

$$\overline{V^C}=\frac{e^2}{4\pi\epsilon_0\epsilon_r\overline{R}}. \tag{8}$$

Here, ϵ_r is the dielectric constant of the quantum-well material. In order to determine the importance of the excitonic interaction, we estimate the ratio of $\overline{V^C}$ to E_F to be

$$\frac{\overline{V^C}}{E_F}=\frac{2}{k_F^2\overline{R}a_B^*}, \tag{9}$$

where $a_B^*=4\pi\epsilon_0\epsilon_r\hbar^2/m_We^2$ is the effective Bohr radius of the two-dimensional electron gas in the quantum well. As an example, we choose $\epsilon_r=12$, $m_W=0.067m_0$ for GaAs well material, and $L_W=100$ Å. For $\overline{V^C}=E_F$, we get

$$n_{2D}=\frac{1}{\pi(a_B^*)^2}\sqrt{\frac{4a_B^*}{3L_W}}=4\times10^{11}\ \text{cm}^{-2}, \tag{10}$$

which is within the typical range of required electron density in quantum-well devices. Moreover, the screening of the Coulomb interaction [6] between electrons in the quantum well is known to be proportional to n_{2D}. This explains why we need to consider the Coulomb-interaction effects on intersubband electron transitions in the quantum well.

C. Second-quantization of interacting-electron system

The total Hamiltonian operator for interacting electrons in a quantum well in the absence of an electromagnetic field is written as

$$\hat{\mathcal{H}}(t)=\hat{\mathcal{H}}_0(t)+\hat{\mathcal{V}}_H(t)+\hat{\mathcal{V}}_F(t). \tag{11}$$

By using the creation (annihilation) operator $\hat{C}^\dagger_{j\vec{k}}(t)$ [$\hat{C}_{j\vec{k}}(t)$] for electrons, the free-electron Hamiltonian $\hat{\mathcal{H}}_0(t)$ in Eq. (11) simply takes the form

$$\hat{\mathcal{H}}_0(t)=\sum_{j,\vec{k}}E_j^{(0)}(k)\hat{C}^\dagger_{j\vec{k}}(t)\hat{C}_{j\vec{k}}(t), \tag{12}$$

the Hartree-type interaction is

$$\hat{\mathcal{V}}_H(t)=2\sum_{\vec{k}_1,\vec{k}_2}\sum_{j_1,j_2}V^C_{j_1j_2,j_1j_2}(0)n_{j_2}(k_2,t)\hat{C}^\dagger_{j_1\vec{k}_1}(t)\hat{C}_{j_1\vec{k}_1}(t), \tag{13}$$

and the Fock-type interaction is

$$\hat{\mathcal{V}}_F(t)=\frac{1}{2}\sum_{\vec{k}_1,\vec{k}_2}\sum_{\vec{q}\neq0}\sum_{j_1j_2,j_3j_4}V^C_{j_1j_2,j_4j_3}(q)\hat{C}^\dagger_{j_1\vec{k}_1+\vec{q}}(t)\times\hat{C}^\dagger_{j_2\vec{k}_2-\vec{q}}(t)\hat{C}_{j_3\vec{k}_2}(t)\hat{C}_{j_4\vec{k}_1}(t). \tag{14}$$

Here, $n_j(k,t)$ is the occupation probability for electrons in the jth subband with wave vector $\vec{k}$. We have defined the Coulomb interaction matrix in Eqs. (13) and (14) by

$$V^{\mathrm{C}}_{j_1 j_2, j_4 j_3}(q) = \frac{e^2}{2\epsilon_0 \epsilon_{\mathrm{r}} \mathcal{A}[q + q_{\mathrm{TF}}(t)\mathcal{F}(q)]} \times \int_{-\infty}^{+\infty} dz \int_{-\infty}^{+\infty} dz' \phi^*_{j_1}(z)\phi^*_{j_2}(z') \times \exp(-q|z-z'|)\phi_{j_4}(z)\phi_{j_3}(z'), \quad (15)$$

where $\mathcal{A}$ is the cross-sectional area of the quantum-well sample and $1/q_{\mathrm{TF}}(t)$ is the so-called Thomas-Fermi screening length [6] resulting from a two-dimensional electron gas. Under the electric quantum limit (i.e., only the ground state is occupied), $q_{\mathrm{TF}}(t)$ is given by

$$q_{\mathrm{TF}}(t) = \left(\frac{e^2}{2\pi\epsilon_0\epsilon_{\mathrm{r}}}\right) \int_0^{+\infty} k dk \left[-\frac{\partial}{\partial E_1(k,t)} n_1(k,t) \right]. \quad (16)$$

In Eq. (15), the form factor due to finite-size quantization is found to be [6]

$$\mathcal{F}(q) = \int_{-\infty}^{+\infty} dz \int_{-\infty}^{+\infty} dz' |\phi_1(z)|^2 \exp(-q|z-z'|)|\phi_1(z')|^2. \quad (17)$$

The time dependence in the screening length $1/q_{\mathrm{TF}}(t)$ makes the Coulomb interaction $V^{\mathrm{C}}_{j_1 j_2, j_4 j_3}(q)$ between electrons rely on time.

D. Mean-field theory

In the following, we introduce the mean-field approximation to the four-operator term in Eq. (14), which leads us to

$$\hat{C}^\dagger_{j_1\vec{k}_1+\vec{q}}(t)\hat{C}^\dagger_{j_2\vec{k}_2-\vec{q}}(t)\hat{C}_{j_3\vec{k}_2}(t)\hat{C}_{j_4\vec{k}_1}(t)\|_{\vec{q}\neq 0} \approx -\langle\langle \hat{C}^\dagger_{j_1\vec{k}_1+\vec{q}}(t)\hat{C}_{j_3\vec{k}_2}(t)\rangle\rangle \hat{C}^\dagger_{j_2\vec{k}_2-\vec{q}}(t)\hat{C}_{j_4\vec{k}_1}(t)\,\delta_{\vec{k}_1+\vec{q},\vec{k}_2} - \langle\langle \hat{C}^\dagger_{j_2\vec{k}_2-\vec{q}}(t)\hat{C}_{j_4\vec{k}_1}(t)\rangle\rangle \hat{C}^\dagger_{j_1\vec{k}_1+\vec{q}}(t)\hat{C}_{j_3\vec{k}_2}(t)\,\delta_{\vec{k}_2-\vec{q},\vec{k}_1}. \quad (18)$$

Under the mean-field approximation, the total Hamiltonian operator in Eq. (11), including an additional interaction with a uniform electromagnetic field, can be simplified as

$$\hat{\mathcal{H}}(t) = \sum_{j,\vec{k}} E^{(0)}_j(k,t)\hat{\sigma}_{jj}(k,t) - \sum_{j,j';\vec{k}}^{j\neq j'} \Delta_{jj'}(k,t)\hat{\sigma}_{jj'}(k,t) + \sum_{j,j';\vec{k}} \mathcal{S}_{jj'}(t)\hat{\sigma}_{jj'}(k,t). \quad (19)$$

Here, $\hat{\sigma}_{jj'}(k,t) = \hat{C}^\dagger_{j\vec{k}}(t)\hat{C}_{j'\vec{k}}(t)$. In Eq. (19), the quasiparticle-renormalized kinetic energy under the mean-field approximation is

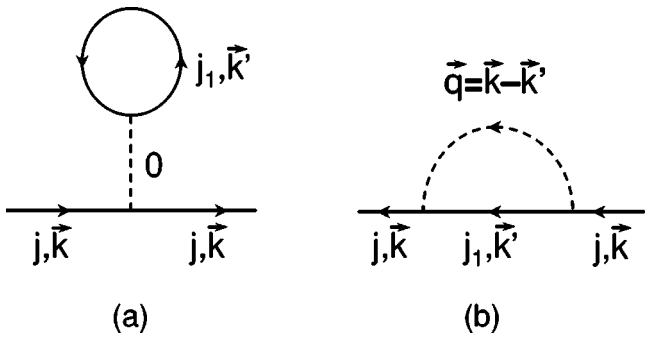

FIG. 1. Feynman diagrams in momentum space for the Hartree (a) and Fock (b) approximations used for the second and third terms in Eq. (20). Here, the solid straight lines with an arrow represent the Green's function for noninteracting conduction electrons and the dashed lines stand for the Coulomb potential between two electrons. The labels j, j_1 are the subband indexes, $\mathbf{k}, \mathbf{k}'$ are the wave vectors of electrons, and $\mathbf{q}$ is the wave vector of the Coulomb potential.

$$E_j(k,t) = E^{(0)}_j(k) + 2\sum_{j_1,\vec{k}'} V^{\mathrm{C}}_{jj_1,jj_1}(0)n_{j_1}(k',t) - \sum_{j_1,\vec{k}'}^{\vec{k}'\neq\vec{k}} V^{\mathrm{C}}_{jj_1,j_1 j}(|\vec{k}-\vec{k}'|)n_{j_1}(k',t), \quad (20)$$

and the quasiparticle-renormalized dipole-coupling energy becomes

$$\Delta_{jj'}(k,t) = e\mathcal{E}_{\mathrm{L}}(t)\int_{-\infty}^{+\infty} dz\, \phi^*_j(z) z \phi_{j'}(z) - \sum_{\vec{k}'}^{\vec{k}'\neq\vec{k}} \sum_{j_1,j_3}^{j_1\neq j_3} V^{\mathrm{C}}_{jj_1,j_3 j'}(|\vec{k}-\vec{k}'|)\rho_{j_3 j_1}(k',t), \quad (21)$$

where $\mathcal{E}_{\mathrm{L}}(t)$ is the time-dependent amplitude of a spatially uniform electromagnetic field. Equations (20) and (21) result from a quasiparticle theory which includes renormalization of both kinetic energy and dipole coupling to an external electromagnetic field. The second and third interaction terms in Eq. (20) are illustrated by Feynman diagrams in Figs. 1(a) and 1(b), respectively. $\mathcal{S}_{jj'}(t)$ in Eq. (19) represents the screening effect in the long-wavelength limit, i.e., $q\to 0$. By using the self-consistent-field approach [6], $\mathcal{S}_{jj'}(t)$ is given by

$$\mathcal{S}_{jj'}(t) = 2\sum_{m,n}^{m\neq n} \sum_{\vec{k}'} \rho_{mn}(k',t)V^{\mathrm{C}}_{jn,j'm}(0), \quad (22)$$

which generates a so-called depolarization shift of absorption peaks [8]. Here, $\rho_{mn}(k,t)$ for $m\neq n$ is the off-diagonal density-matrix element representing an optically induced polarization of the electron-gas system.

E. Many-body density-matrix equations

By introducing a statistical average to $\hat{\sigma}_{j'j}(k,t)$ through a density operator $\hat{\rho}(t)$ of the system, we get the density-matrix elements

$$\rho_{jj'}(k,t)=\langle\langle\hat{\sigma}_{j'j}(k,t)\rangle\rangle\equiv \mathrm{Tr}\{\hat{\sigma}_{j'j}(k,t)\hat{\rho}(t)\}. \tag{23}$$

The equation-of-motion for the operator $\hat{\sigma}_{j'j}(k,t)$ [1] leads us to the following density-matrix equations for $j\neq j'$ (optically-induced polarization):

$$\frac{\partial}{\partial t}\rho_{jj'}(k,t)=\frac{1}{i\hbar}\sum_m [\mathcal{H}_{jm}(t)\rho_{mj'}(k,t)-\rho_{jm}(k,t)\mathcal{H}_{mj'}(t)] - \frac{1}{2}(\gamma_j+\gamma_{j'})\rho_{jj'}(k,t), \tag{24}$$

where γ_j is the homogeneous broadening of jth subband due to electron scattering and $\mathcal{H}_{jm}(t)$ is the matrix elements of the Hamiltonian operator in Eq. (19). For $j=j'$ (occupation probability), we have

$$\frac{\partial}{\partial t}\rho_{jj}(k,t)\equiv\frac{\partial}{\partial t}n_j(k,t)=-\frac{2}{\hbar}\sum_m \mathrm{Im}[\rho_{jm}(k,t)\mathcal{H}_{mj}(t)]. \tag{25}$$

Substituting Eq. (19) into Eq. (25) in the presence of the strong electromagnetic field, we get

$$\frac{\partial}{\partial t}n_j(k,\omega_{\mathrm{L}};t)=\frac{2}{\hbar}\sum_m^{m\neq j}\mathrm{Im}[\Delta_{mj}(k,t)\rho_{jm}(k,\omega_{\mathrm{L}};t)], - \frac{4}{\hbar}\sum_m^{m\neq j}\mathrm{Im}\left\{\rho_{jm}(k,\omega_{\mathrm{L}};t)\times\sum_{k'}\left[\sum_{i,i'}^{i\neq i'}\rho_{ii'}(k',\omega_{\mathrm{L}};t)V^{\mathrm{C}}_{mi',ji}(0)\right]\right\}, \tag{26}$$

which leads to

$$\frac{\partial}{\partial t}\sum_j n_j(k,\omega_{\mathrm{L}};t)\equiv 0.$$

Inserting Eq. (19) into Eq. (24), we find

$$\begin{aligned}\frac{\partial}{\partial t}\rho_{jj'}(k,\omega_{\mathrm{L}};t)=&-\frac{1}{2}(\gamma_j+\gamma_{j'})\rho_{jj'}(k,\omega_{\mathrm{L}};t)+\frac{1}{i\hbar}[E_j(k,t)-E_{j'}(k,t)+\hbar\omega_{\mathrm{L}}]\rho_{jj'}(k,\omega_{\mathrm{L}};t)\\ &-\frac{1}{i\hbar}\sum_m^{m\neq j}\Delta_{jm}(k,t)\rho_{mj'}(k,\omega_{\mathrm{L}};t)\\ &+\frac{1}{i\hbar}\sum_m^{m\neq j'}\Delta_{mj'}(k,t)\rho_{jm}(k,\omega_{\mathrm{L}};t)+\frac{2}{i\hbar}\rho_{jj'}(k,\omega_{\mathrm{L}};t)\sum_{k'}\left\{\sum_{i,\,i'}^{i\neq i'}\rho_{ii'}(k',\omega_{\mathrm{L}};t)[V^{\mathrm{C}}_{ji',ji}(0)-V^{\mathrm{C}}_{j'i',j'i}(0)]\right\}\\ &+\frac{2}{i\hbar}\sum_m^{m\neq j}\rho_{mj'}(k,\omega_{\mathrm{L}};t)\sum_{k'}\left\{\sum_{i,i'}^{i\neq i'}\rho_{ii'}(k',\omega_{\mathrm{L}};t)V^{\mathrm{C}}_{ji',mi}(0)\right\}-\frac{2}{i\hbar}\sum_m^{m\neq j'}\rho_{jm}(k,\omega_{\mathrm{L}};t)\\ &\times\sum_{k'}\left\{\sum_{i,i'}^{i\neq i'}\rho_{ii'}(k',\omega_{\mathrm{L}};t)V^{\mathrm{C}}_{mi',j'i}(0)\right\},\end{aligned} \tag{27}$$

where ω_{L} is the frequency of the electromagnetic field.

F. Quantum-interference effect

In the following, we limit ourselves to a three-level model for the resonant asymmetric double quantum wells, as displayed in Fig. 2. In this double-quantum-well system, the deep/narrow left quantum well has two confined states labeled by $E_{1\mathrm{L}}$ and $E_{2\mathrm{L}}$, and the shallow/wide right quantum well has only one confined state labeled by $E_{1\mathrm{R}}$. There exists a resonant coupling between energy levels $E_{2\mathrm{L}}$ and $E_{1\mathrm{R}}$ due to their alignment in energies. The resonant coupling creates a doublet from these two degenerate energy levels. The doublet is labeled by $E_2^{(0)}(k)$ and $E_3^{(0)}(k)$. Moreover, we denote $E_{1\mathrm{L}}$ by $E_1^{(0)}(k)$ and assume that $E_3^{(0)}(k)-E_2^{(0)}(k)\ll E_2^{(0)}(k)-E_1^{(0)}(k)$. To excite an intersubband transition of electrons in quantum wells, one requires a nonzero component of the incident electromagnetic field along the growth (z) direction. The other component of a *spatially uniform* incident field does not directly interact (dipole coupling) with electrons in

quantum wells. For this reason, an incident electromagnetic field is assumed to be polarized in the z direction with photon energy $\hbar\omega_{\mathrm{L}}$ close to $E_2^{(0)}(k)-E_1^{(0)}(k)$.

By combining the previously derived density-matrix equations [1] in the presence of off-diagonal radiative-decay coupling for noninteracting electrons and Eqs. (26) and (27) for interacting electrons, after the rotating-wave approximation [1] we obtain the following:

$$\frac{d}{dt}n_1(k,\omega_{\mathrm{L}};t)=\frac{2}{\tau_2(k,t)}n_2(k,\omega_{\mathrm{L}};t)+2\beta_{31,13}[\Omega_{31}(k,t)]n_3(k,\omega_{\mathrm{L}};t)+\frac{2}{\hbar}\mathrm{Im}[\Delta_{12}^*(k,t)\rho_{12}(k,\omega_{\mathrm{L}};t)+\Delta_{13}^*(k,t)\rho_{13}(k,\omega_{\mathrm{L}};t)]$$
$$+2\{\beta_{31,12}[\Omega_{21}(k,t)]+\beta_{21,13}[\Omega_{31}(k,t)]\}\mathrm{Re}[\rho_{23}(k,\omega_{\mathrm{L}};t)]-\frac{4}{\hbar}\sum_{\vec{k}'}\mathrm{Im}\{\rho_{12}(k,\omega_{\mathrm{L}};t)$$
$$\times[\rho_{12}^*(k',\omega_{\mathrm{L}};t)V_{21,12}^{\mathrm{C}}(0)+\rho_{13}^*(k',\omega_{\mathrm{L}};t)V_{21,13}^{\mathrm{C}}(0)]\}-\frac{4}{\hbar}\sum_{\vec{k}'}\mathrm{Im}\{\rho_{13}(k,\omega_{\mathrm{L}};t)[\rho_{12}^*(k',\omega_{\mathrm{L}};t)V_{31,12}^{\mathrm{C}}(0)$$
$$+\rho_{13}^*(k',\omega_{\mathrm{L}};t)V_{31,13}^{\mathrm{C}}(0)]\}, \tag{28}$$

$$\frac{d}{dt}n_2(k,\omega_{\mathrm{L}};t)=-\frac{2}{\tau_2(k,t)}n_2(k,\omega_{\mathrm{L}};t)+2\beta_{32,23}[\Omega_{32}(k,t)]n_3(k,\omega_{\mathrm{L}};t)-\frac{2}{\hbar}\mathrm{Im}[\Delta_{12}^*(k,t)\rho_{12}(k,\omega_{\mathrm{L}};t)+\Delta_{23}(k,t)\rho_{23}^*(k,\omega_{\mathrm{L}};t)]$$
$$-2\beta_{21,13}[\Omega_{31}(k,t)]\mathrm{Re}[\rho_{23}(k,\omega_{\mathrm{L}};t)]-\frac{4}{\hbar}\sum_{\vec{k}'}\mathrm{Im}\{\rho_{12}^*(k,\omega_{\mathrm{L}};t)[\rho_{12}(k',\omega_{\mathrm{L}};t)V_{12,21}^{\mathrm{C}}(0)$$
$$+\rho_{13}(k',\omega_{\mathrm{L}};t)V_{13,21}^{\mathrm{C}}(0)]\}-\frac{4}{\hbar}\sum_{\vec{k}'}\mathrm{Im}\{\rho_{23}(k,\omega_{\mathrm{L}};t)[\rho_{23}(k',\omega_{\mathrm{L}};t)V_{33,22}^{\mathrm{C}}(0)+\rho_{23}^*(k',\omega_{\mathrm{L}};t)V_{32,23}^{\mathrm{C}}(0)]\}, \tag{29}$$

$$\frac{d}{dt}\rho_{12}(k,\omega_{\mathrm{L}};t)=-\frac{1}{2}(\gamma_1+\gamma_2)\rho_{12}(k,\omega_{\mathrm{L}};t)+i[\Omega_{21}(k,t)-\omega_{\mathrm{L}}]\rho_{12}(k,\omega_{\mathrm{L}};t)-\frac{1}{\tau_2(k,t)}\rho_{12}(k,\omega_{\mathrm{L}};t)+\frac{i}{\hbar}\Delta_{12}(k,t)[n_2(k,\omega_{\mathrm{L}};t)$$
$$-n_1(k,\omega_{\mathrm{L}};t)]+\frac{i}{\hbar}\Delta_{13}(k,t)\rho_{23}^*(k,\omega_{\mathrm{L}};t)-\frac{i}{\hbar}\Delta_{23}^*(k,t)\rho_{13}(k,\omega_{\mathrm{L}};t)-\beta_{21,13}[\Omega_{31}(k,t)]\rho_{13}(k,\omega_{\mathrm{L}};t)$$
$$-\frac{2i}{\hbar}\rho_{12}(k,\omega_{\mathrm{L}};t)\sum_{\vec{k}'}\{\rho_{23}(k',\omega_{\mathrm{L}};t)[V_{13,12}^{\mathrm{C}}(0)-V_{23,22}^{\mathrm{C}}(0)]+\rho_{23}^*(k',\omega_{\mathrm{L}};t)[V_{12,13}^{\mathrm{C}}(0)-V_{22,23}^{\mathrm{C}}(0)]\}$$
$$-\frac{2i}{\hbar}n_2(k,\omega_{\mathrm{L}};t)\sum_{\vec{k}'}[\rho_{12}(k',\omega_{\mathrm{L}};t)V_{12,21}^{\mathrm{C}}(0)+\rho_{13}(k',\omega_{\mathrm{L}};t)V_{13,21}^{\mathrm{C}}(0)]$$
$$-\frac{2i}{\hbar}\rho_{23}^*(k,\omega_{\mathrm{L}};t)\sum_{\vec{k}'}[\rho_{12}(k',\omega_{\mathrm{L}};t)V_{12,31}^{\mathrm{C}}(0)+\rho_{13}(k',\omega_{\mathrm{L}};t)V_{13,31}^{\mathrm{C}}(0)]$$
$$+\frac{2i}{\hbar}n_1(k,\omega_{\mathrm{L}};t)\sum_{\vec{k}'}[\rho_{12}(k',\omega_{\mathrm{L}};t)V_{12,21}^{\mathrm{C}}(0)+\rho_{13}(k',\omega_{\mathrm{L}};t)V_{13,21}^{\mathrm{C}}(0)]$$
$$+\frac{2i}{\hbar}\rho_{13}(k,\omega_{\mathrm{L}};t)\sum_{\vec{k}'}[\rho_{23}(k',\omega_{\mathrm{L}};t)V_{33,22}^{\mathrm{C}}(0)+\rho_{23}^*(k',\omega_{\mathrm{L}};t)V_{32,23}^{\mathrm{C}}(0)], \tag{30}$$

$$\frac{d}{dt}\rho_{13}(k,\omega_{\mathrm{L}};t)=-\frac{1}{2}(\gamma_1+\gamma_3)\rho_{13}(k,\omega_{\mathrm{L}};t)+i[\Omega_{31}(k,t)-\omega_{\mathrm{L}}]\rho_{13}(k,\omega_{\mathrm{L}};t)-\frac{1}{\tau_3(k,t)}\rho_{13}(k,\omega_{\mathrm{L}};t)+\frac{i}{\hbar}\Delta_{13}(k,t)[n_3(k,\omega_{\mathrm{L}};t)$$
$$-n_1(k,\omega_{\mathrm{L}};t)]+\frac{i}{\hbar}\Delta_{12}(k,t)\rho_{23}(k,\omega_{\mathrm{L}};t)-\frac{i}{\hbar}\Delta_{23}(k,t)\rho_{12}(k,\omega_{\mathrm{L}};t)-\beta_{31,12}[\Omega_{21}(k,t)]\rho_{12}(k,\omega_{\mathrm{L}};t)$$
$$-\frac{2i}{\hbar}\rho_{13}(k,\omega_{\mathrm{L}};t)\sum_{\vec{k}'}\{\rho_{23}(k',\omega_{\mathrm{L}};t)[V_{13,12}^{\mathrm{C}}(0)-V_{33,32}^{\mathrm{C}}(0)]+\rho_{23}^*(k',\omega_{\mathrm{L}};t)[V_{12,13}^{\mathrm{C}}(0)-V_{32,33}^{\mathrm{C}}(0)]\}$$

$$-\frac{2i}{\hbar}\rho_{23}(k,\omega_L;t)\sum_{\vec{k}'}[\rho_{12}(k',\omega_L;t)V^C_{12,21}(0)+\rho_{13}(k',\omega_L;t)V^C_{13,21}(0)]$$

$$-\frac{2i}{\hbar}n_3(k,\omega_L;t)\sum_{\vec{k}'}[\rho_{12}(k',\omega_L;t)V^C_{12,31}(0)+\rho_{13}(k',\omega_L;t)V^C_{13,31}(0)]$$

$$+\frac{2i}{\hbar}n_1(k,\omega_L;t)\sum_{\vec{k}'}[\rho_{12}(k',\omega_L;t)V^C_{12,31}(0)+\rho_{13}(k',\omega_L;t)V^C_{13,31}(0)]$$

$$+\frac{2i}{\hbar}\rho_{12}(k,\omega_L;t)\sum_{\vec{k}'}[\rho_{23}(k',\omega_L;t)V^C_{23,32}(0)+\rho^*_{23}(k',\omega_L;t)V^C_{22,33}(0)], \tag{31}$$

$$\frac{d}{dt}\rho_{23}(k,\omega_L;t)=-\frac{1}{2}(\gamma_2+\gamma_3)\rho_{23}(k,\omega_L;t)+i\Omega_{32}(k,t)\rho_{23}(k,\omega_L;t)-\left[\frac{1}{\tau_2(k,t)}+\frac{1}{\tau_3(k,t)}\right]\rho_{23}(k,\omega_L;t)+\frac{i}{\hbar}\Delta_{23}(k,t)$$

$$\times[n_3(k,\omega_L;t)-n_2(k,\omega_L;t)]+\frac{i}{\hbar}\Delta^*_{12}(k,t)\rho_{13}(k,\omega_L;t)-\frac{i}{\hbar}\Delta_{13}(k,t)\rho^*_{12}(k,\omega_L;t)$$

$$+\beta_{23,23}[\Omega_{32}(k,t)]\rho^*_{23}(k,\omega_L;t)-\{\beta_{21,13}[\Omega_{31}(k,t)]n_3(k,\omega_L;t)+\beta_{31,12}[\Omega_{21}(k,t)]n_2(k,\omega_L;t)\}$$

$$-\frac{2i}{\hbar}\rho_{23}(k,\omega_L;t)\sum_{\vec{k}'}\{\rho_{23}(k',\omega_L;t)[V^C_{23,22}(0)-V^C_{33,32}(0)]+\rho^*_{23}(k',\omega_L;t)[V^C_{22,23}(0)-V^C_{32,33}(0)]\}$$

$$-\frac{2i}{\hbar}\rho_{13}(k,\omega_L;t)\sum_{\vec{k}'}[\rho^*_{12}(k',\omega_L;t)V^C_{21,12}(0)+\rho^*_{13}(k',\omega_L;t)V^C_{21,13}(0)]$$

$$-\frac{2i}{\hbar}n_3(k,\omega_L;t)\sum_{\vec{k}'}[\rho_{23}(k',\omega_L;t)V^C_{23,32}(0)+\rho^*_{23}(k',\omega_L;t)V^C_{22,33}(0)]$$

$$+\frac{2i}{\hbar}\rho^*_{12}(k,\omega_L;t)\sum_{\vec{k}'}[\rho_{12}(k',\omega_L;t)V^C_{12,31}(0)+\rho_{13}(k',\omega_L;t)V^C_{13,31}(0)]$$

$$+\frac{2i}{\hbar}n_2(k,\omega_L;t)\sum_{\vec{k}'}[\rho_{23}(k',\omega_L;t)V^C_{23,32}(0)+\rho^*_{23}(k',\omega_L;t)V^C_{22,33}(0)], \tag{32}$$

where $\hbar\Omega_{ij}(k,t)=E_i(k,t)-E_j(k,t)$ with

$$E_j(k,t)=E^{(0)}_j(k)+2\sum_{j_1,\vec{k}'}V^C_{jj_1,jj_1}(0)n_{j_1}(k',\omega_L;t)$$

$$-\sum_{j_1,\vec{k}'}^{\vec{k}'\neq\vec{k}}V^C_{jj_1,j_1j}(|\vec{k}-\vec{k}'|)n_{j_1}(k',\omega_L;t). \tag{33}$$

For $j<j'$ [excluding $\Delta_{23}(k,t)$] we get

$$\Delta_{jj'}(k,t)=e\mathcal{E}_L(t)\int_{-\infty}^{+\infty}dz\,\phi^*_j(z)z\phi_{j'}(z)$$

$$-\sum_{\vec{k}'}^{\vec{k}'\neq\vec{k}}[V^C_{j2,1j'}(|\vec{k}-\vec{k}'|)\rho_{12}(k',\omega_L;t)$$

$$+V^C_{j3,1j'}(|\vec{k}-\vec{k}'|)\rho_{13}(k',\omega_L;t)], \tag{34}$$

and

$$\Delta_{23}(k,t)=-\sum_{\vec{k}'}^{\vec{k}'\neq\vec{k}}[V^C_{22,33}(|\vec{k}-\vec{k}'|)\rho^*_{23}(k',\omega_L;t)$$

$$+V^C_{23,23}(|\vec{k}-\vec{k}'|)\rho_{23}(k',\omega_L;t)], \tag{35}$$

while for $j>j'$ we have $\Delta_{jj'}(k,t)=\Delta^*_{j'j}(k,t)$. In Eqs. (28)–(32), we have defined the radiative-decay rate for subbands with $j=1,2,3$ by [1]

$$\frac{1}{\tau_j(k,t)}=\sum_{i<j}\beta_{ji,ij}[\Omega_{ji}(k,t)]. \tag{36}$$

Here, $\beta_{jj',ii'}[\Omega_{i'i}(k,t)]$ in Eqs. (28)–(32) and (36) is the real part of the radiative-decay coupling matrix elements, given by [1]

$$\beta_{jj',ii'}[\Omega_{i'i}(k,t)]=\frac{2e^2\Omega^3_{i'i}(k,t)}{3\hbar\epsilon_0\epsilon_r c^3}\theta[\Omega_{i'i}(k,t)]d_{jj'}d_{ii'}, \tag{37}$$

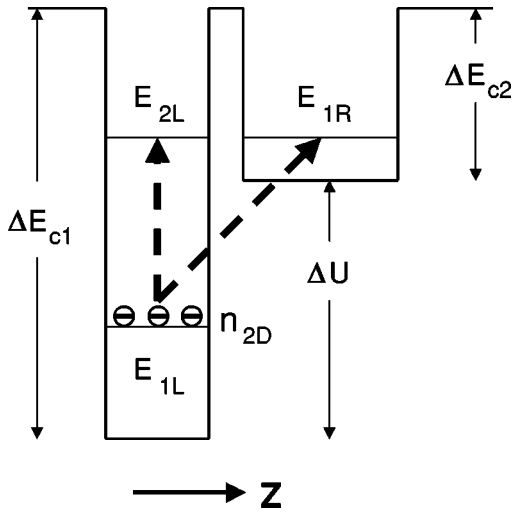

FIG. 2. Illustration of three-level resonant asymmetric double quantum wells with intersubband field coupling. The barrier material is $Al_{0.35}Ga_{0.65}As$, and the materials for the left and right wells are GaAs and $Al_{0.208}Ga_{0.792}As$, respectively. Two degenerate electron transitions in the system are indicated by the thick dashed arrows. L_{W1} and L_{W2} are the widths of the left and right wells, and L_B is the thickness of the middle barrier. ΔE_{c1} and ΔE_{c2} are the conduction-band offsets for the left and right wells, and ΔU is the step height between the bottoms of the two wells. The electromagnetic field $\mathcal{E}_L(t)$ is assumed to be polarized in the z direction. The lower-energy state in the left well contains electron density n_{2D} illustrated by three circles filled with "$-$" signs at their centers. All the parameters for this sample are summarized in Tables I and II.

where $\theta(x)$ is the Heaviside step function and

$$d_{jj'}=\int_{-\infty}^{+\infty} dz\,\phi_j^*(z)z\,\phi_{j'}(z). \tag{38}$$

From Eq. (37) we obtain the *diagonal* radiative-decay rate $\beta_{ji,ij}[\Omega_{i'i}(k,t)]$ for $j>i$ when $j'=i$ and $i'=j$. The rest of the *off-diagonal* radiative-decay rates reflect the coupling between two optical transitions, i.e., from level j' to j and from level i' to i. The quantum-interference effect is taken into consideration by including $\beta_{21,13}[\Omega_{21}(k,t)]$ and $\beta_{31,12}[\Omega_{21}(k,t)]$ terms in Eqs. (30) and (31), respectively [1]. The scaled density for electrons in jth subband is calculated as

$$N_j(\omega_L,t)=\frac{2}{n_{2D}}\sum_k n_j(k,\omega_L;t). \tag{39}$$

G. Dielectric function and optical absorption

Based on the calculated density-matrix elements, the statistically averaged polarization (per unit volume) of the system can be found from

$$\mathcal{P}(\omega_L;t)=-\left(\frac{1}{L_z\mathcal{A}\mathcal{E}_L(t)}\right)\sum_k \Delta_{12}^*(k,t)\rho_{12}(k,\omega_L;t) + \Delta_{13}^*(k,t)\rho_{13}(k,\omega_L;t)+\Delta_{23}^*(k,t)\rho_{23}(k,\omega_L;t)], \tag{40}$$

TABLE I. Conduction-band offsets $\Delta E_{c1}/\Delta E_{c2}$, step height ΔU, well widths L_{W1}/L_{W2}, middle barrier thickness L_B, and electron density n_{2D} for samples 1 and 2 shown in Fig. 2 with different electron densities.

Sample no.	$\Delta E_{c1}/\Delta E_{c2}$ (meV)	ΔU (meV)	L_{W1}/L_{W2} (Å)	L_B (Å)	n_{2D} ($\times 10^{11}$cm^{-2})
1	249/101	148	75/85	50	0.8
2	249/101	148	75/85	50	1.6

where L_z is the total length of the double quantum wells. Using Eq. (40) we get the Lorentz ratio (polarizability) as [6]

$$\chi(\omega_L;t)=\frac{\mathcal{P}(\omega_L;t)}{\epsilon_0\mathcal{E}_L(t)} =-\left(\frac{1}{\epsilon_0 L_z\mathcal{A}\mathcal{E}_L^2(t)}\right)\sum_k [\Delta_{12}^*(k,t)\rho_{12}(k,\omega_L;t) + \Delta_{13}^*(k,t)\rho_{13}(k,\omega_L;t)+\Delta_{23}^*(k,t)\rho_{23}(k,\omega_L;t)\}, \tag{41}$$

which becomes independent of $\mathcal{E}_L(t)$ under the weak-field limit $[\mathcal{E}_L(t)\to 0]$. The time-dependent complex dielectric function can be calculated from the Lorentz ratio [6],

$$\epsilon(\omega_L;t)=\epsilon_r+\chi(\omega_L;t). \tag{42}$$

The absorption coefficient is found to be [6]

$$\alpha(\omega_L;t)=\frac{\omega_L}{n(\omega_L;t)c}[N_{ph}(\omega_L)+1]\mathrm{Im}[\chi(\omega_L;t)], \tag{43}$$

where $N_{ph}(\omega_L)=1/[\exp(\hbar\omega_L/k_BT)-1]$ is the Bose function for incident photons and the refractive-index function in Eq. (43) is given by

$$n(\omega_L;t)=\frac{1}{\sqrt{2}}\{\epsilon_r+\mathrm{Re}[\chi(\omega_L;t)] + \sqrt{\{\epsilon_r+\mathrm{Re}[\chi(\omega_L;t)]\}^2+\{\mathrm{Im}[\chi(\omega_L;t)]\}^2}\}^{1/2}. \tag{44}$$

In Eq. (43), $\alpha(\omega_L;t)>0$ indicates photon absorption by electrons in quantum wells while $\alpha(\omega_L;t)<0$ corresponds to a gain for the external electromagnetic field provided by electrons in the quantum wells.

III. NUMERICAL RESULTS AND DISCUSSION

In this section, we present the steady-state optical spectra for resonant asymmetric double quantum wells with intersubband coupling (see Fig. 2). For the samples used in our numerical study, the barrier material is $Al_{0.35}Ga_{0.65}As$ and the materials for the left and right quantum wells are GaAs and $Al_{0.208}Ga_{0.792}As$, respectively. The electron density in the quantum wells is denoted as n_{2D}. There are two confined electron states in the left quantum well, indicated by E_{1L} and

TABLE II. Calculated single-well electron energy levels $E_{1L}=E_1$ and E_{2L} in the left quantum well and E_R in the right well for the sample shown in Fig. 2, as well as the energy levels of the tunneling-split doublet E_2 and E_3.

$E_{1L}=E_1$ (meV)	E_{2L} (meV)	E_{1R} (meV)	E_2 (meV)	E_3 (meV)
45	173	173	170	176

E_{2L}, and one confined electron state in the right quantum well, denoted by E_{1R}. The sample parameters and the calculated energy levels in the left and right quantum wells are summarized in Tables I and II. The upper energy level in the left quantum well is aligned with the energy level in the right quantum well, producing a tunneling-split doublet. The strong external electromagnetic field applied to the system is polarized in the *z* direction. The frequency of the electromagnetic field is set close to the energy separation between the lower level in the left quantum well and the doublet. As a result, the three-level model for the intersubband-coupled quantum wells [1] can be adopted here after the inclusion of Coulomb-interaction effects.

In our calculation, we have taken $T=4$ K, $\mathcal{E}_L=20$ kV/cm (equivalent to 2 W for this field strength), average dielectric constant $\epsilon_r=12$, and $\gamma_j=\gamma_0$ for $j=1$, 2, 3. For the left (right) well, we have found $\Delta_0=0.341$ (0.333) eV, $E_p=22.71$ (20.50) eV, $E_G=1.52$ (1.78) eV, and $\Delta E_{c1}=248.77$ meV for the barrier height of the left well. The chemical potential of the noninteracting-electron gas is calculated to be $\mu(n_{2D},T)-E_1=2.75$ (5.50) meV at $T=4$ K for sample 1 (2). In addition, we take $\gamma_0/\beta^{(0)}_{21,12}=5$ at $k=0$ for Figs. 3–6 and vary this ratio in Fig. 7, and $\beta^{(0)}_{21,12}$ is defined in Eq. (37) for single-particle energy-level separation $\hbar\Omega^{(0)}_{21}$.

Figure 3 presents the ratios of quasiparticle off-diagonal radiative-decay coupling rates for sample 1 from many-body density-matrix theory including the quantum-interference effect. It is clear from the figure that $\beta_{31,12}/\beta^{(0)}_{31,12}$, $\beta_{21,13}/\beta^{(0)}_{21,13}<1$. This reflects the reduction of the quantum-interference effect by the quasiparticle renormalization. We note that the Hartree-energy correction to the first subband is

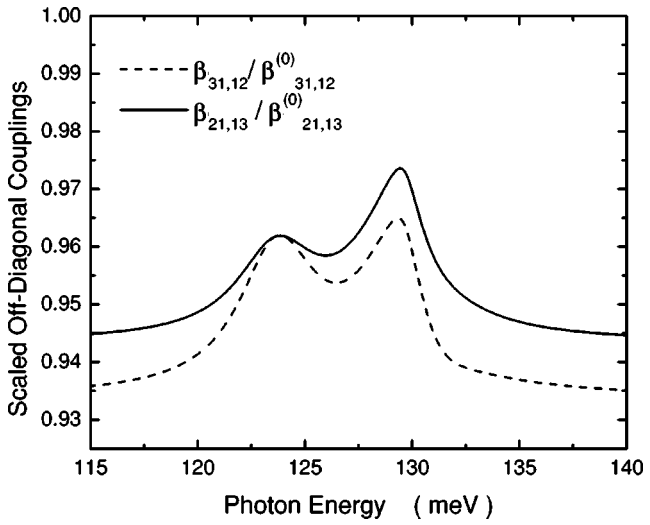

FIG. 3. Scaled off-diagonal radiative-decay couplings $\beta_{31,12}/\beta^{(0)}_{31,12}$ (solid curve) and $\beta_{21,13}/\beta^{(0)}_{21,13}$ (dashed curve) at $k=0$ for sample 1 as functions of photon energy $\hbar\omega_L$, where $\beta_{ij,mn}$ and $\beta^{(0)}_{ij,mn}$ represent the quasiparticle and single-particle off-diagonal radiative-decay coupling rates, respectively.

relatively stronger compared to the corrections to the two higher subbands. This leads to a decrease in the energy-level separations. The dependence of the energy-level separations on the photon energy $\hbar\omega_L$ is because the Hartree-energy correction is proportional to the subband density $N_j(\omega_L)$ which depends on $\hbar\omega_L$ through the many-body density-matrix equations. Whenever $N_1(\omega_L)$ reaches either of its two minima [see Fig. 4(b)], the energy-level separations show a peak at the same photon energy due to a reduced Hartree correction to the ground subband (not shown here). Based on these reasons, the decrease of the off-diagonal radiative-decay coupling rates by the Coulomb interaction between electrons can be easily explained since they have a cubic dependence on the energy-level separations, as shown by Eq. (37).

We display in Fig. 4 absorption coefficients $\alpha(\omega_L)$ [in Fig. 4(a)] and scaled first-subband densities $N_1(\omega_L)$ [in Fig. 4(b)] calculated from the many-body density-matrix equa-

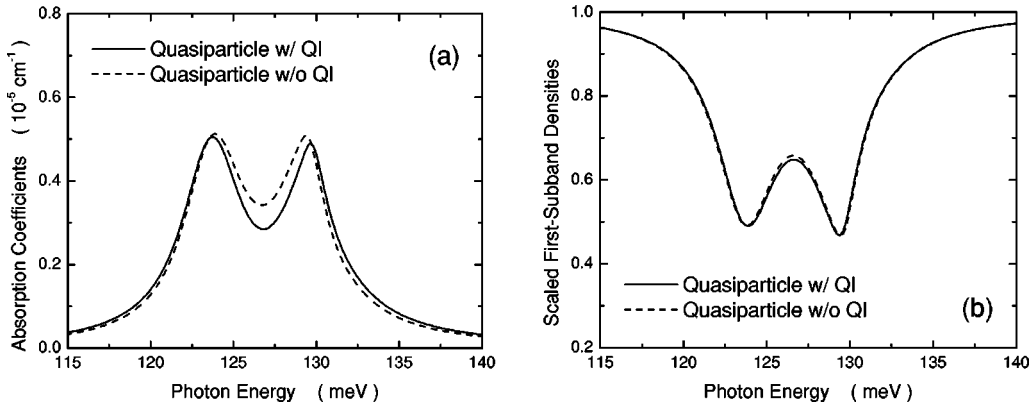

FIG. 4. Calculated absorption coefficient $\alpha(\omega_L)$ (a) and scaled first-subband density $N_1(\omega_L)$ (b) of quasiparticles from the many-body density-matrix equations for the cases with (solid curves) and without (dashed curves) the quantum-interference (QI) effects for sample 1 as functions of $\hbar\omega_L$. Including QI means we take nonzero off-diagonal radiative-decay couplings $\beta_{31,12}$, $\beta_{21,13}$, and $\beta_{23,23}$.

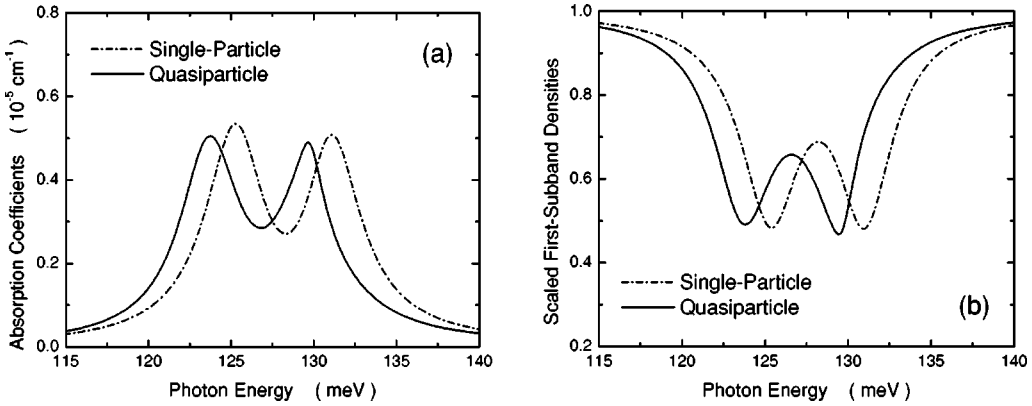

FIG. 5. Calculated $\alpha(\omega_L)$ (a) and $N_1(\omega_L)$ (b) from density-matrix equations which include the quantum-interference effect for the cases of the single-particle theory (solid curves), the quasiparticle theory for sample 1 as functions of $\hbar\omega_L$.

tions for the cases with (solid curves) and without (dashed curves) quantum-interference effects. From Fig. 4(a) we find that the quantum-interference effect deepens the minimum between the two absorption peaks. Moreover, a small asymmetry in the strengths of the two absorption peaks is created by this effect, as it slightly increases the separation between the peaks. The ω_L dependence of $N_1(\omega_L)$ in Fig. 4(b) is correlated to the features found in Fig. 4(a). Whenever there is an absorption peak, there will be a minimum in $N_1(\omega_L)$ at the same photon energy due to transferring electrons from the lowest subband to the upper tunneling-split doublet. The maximum of $N_1(\omega_L)$ between the two minima is reduced slightly by quantum interference. From this figure, we find that the quantum-interference effect predicted for this system [1] is robust against the Coulomb interaction between electrons in the mean-field approximation.

Figure 5 is used to exhibit the Coulomb-interaction effect, where $\alpha(\omega_L)$ [in Fig. 5(a)] and $N_1(\omega_L)$ [in Fig. 5(b)] from single-particle (dash-dotted curves) and quasiparticle (solid curves) theories including the quantum-interference effect are compared. The two absorption peaks in Fig. 5(a) are significantly shifted down in energy by the Coulomb interaction between electrons due to a strong Hartree correction to the first subband as explained in the discussion of Fig. 3. The strengths of the two absorption peaks are also reduced due to a Fock correction to the dipole coupling as can be seen from Eq. (34). The depolarization shift of the absorption peak is expected to be suppressed due to equal subband density in the lowest subband and one of the higher subbands at the photon energy where the peak absorption occurs. The shift down in energy of the two minima in $N_1(\omega_L)$ can clearly be seen from Fig. 5(b) by comparing the two curves.

Both quantum-interference and Coulomb-interaction effects can also affect the refractive-index function $n(\omega_L)$. In Fig. 6 we see that the Z feature observed in $n(\omega_L)$ as a function of $\hbar\omega_L$ is shifted down in energy when the Coulomb-interaction effects are included. At the same time, $n(\omega_L)$ near the photon energies of two absorption peaks is enhanced. On the other hand, we find that the quantum-interference effect slightly increases $n(\omega_L)$ near the photon energy of the lower absorption peak (not shown).

From Fig. 7(a), we find that the minimum between the two absorption peaks becomes more and more insignificant with the increase of γ_0 due to suppression of the quantum-interference effect. Moreover, it is known that the Coulomb-interaction effect depends on the electron density n_{2D}. At the same time, both absorption peaks are broadened with γ_0. From Fig. 7(b), we find that the two absorption peaks are pushed even lower in energy with increased n_{2D} due to an enhanced Hartree correction to the first subband (comparing thin and thick solid curves), but the peak positions are not changed from the single-particle theory (comparing thin and thick dashed curves). In addition, the strengths of the two absorption peaks are increased with n_{2D} due to more electrons being available for intersubband transitions (comparing thin and thick dashed curves). Finally, the enhanced Fock correction to the dipole coupling as n_{2D} is increased tends to reduce the strengths of the absorption peaks even more.

IV. CONCLUSIONS

We have derived many-body density-matrix equations by including quasiparticle renormalization of kinetic energy and

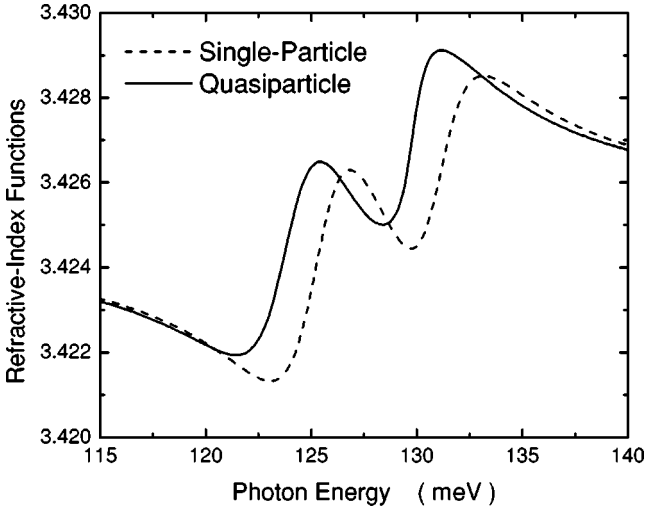

FIG. 6. Calculated refractive-index function $n(\omega_L)$ from the single-particle (dashed curve) and the quasiparticle (solid curve) density-matrix equations including the the quantum-interference effect for sample 1 as functions of $\hbar\omega_L$.

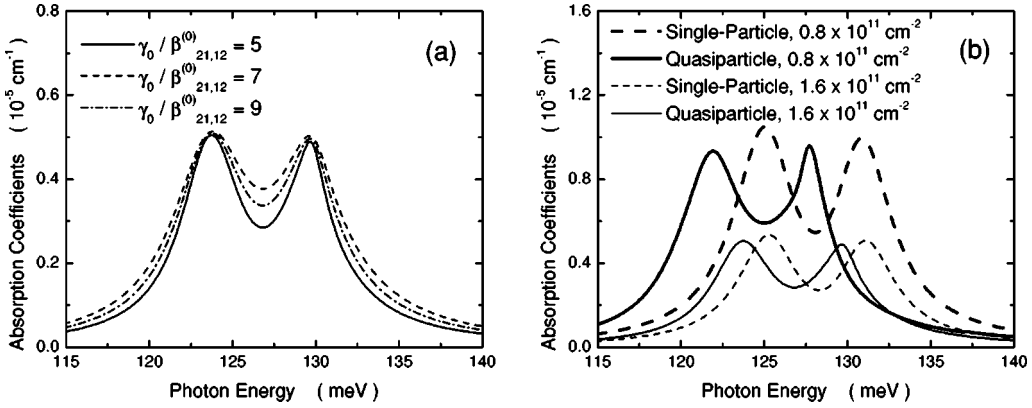

FIG. 7. Calculated $\alpha(\omega_L)$ for different dephasing rates γ_0 in (a) and for comparison between samples 1 and 2 in (b) from density-matrix equations which include the quantum-interference effect. In (a), $\alpha(\omega_L)$ of sample 1 for the case of the quasiparticle theory with $\gamma_0/\beta^{(0)}_{21,12}=5$ (solid curve), 7 (dashed curve) and 9 (dash-dotted curve) at $k=0$ are compared. In (b), $\alpha(\omega_L)$ with $\gamma_0/\beta^{(0)}_{21,12}=5$ at $k=0$ for samples 1 (thick curves) and 2 (thin curves) are compared for the cases of the single-particle theory (dashed curves) and the quasiparticle theory (solid curves).

dipole coupling to a strong electromagnetic field, as well as screening and quantum-interference effects. We have applied these equations to a three-level resonant asymmetric double-quantum-well system in which the ground subband is coupled to the upper tunneling-split doublet by the electromagnetic field. Using these equations, we have calculated the quasiparticle energy-level separations and off-diagonal radiative-decay coupling rates, absorption coefficient, refractive-index function, and scaled subband electron density as functions of incident photon energy. From the calculated results, we have analyzed the role played by quantum interference in the quasiparticle renormalization. The quantum interference in the system has been shown to be robust against the Coulomb interaction between electrons in the mean-field approximation. The effects of dephasing rate and electron density have also been explored.

In this paper, we display numerical results for absorption spectra in steady state, and employ a homogeneous level broadening for the dephasing rate in equations determining off-diagonal density-matrix elements. If one wants to see dynamical effects of Coulomb scattering [7] on quantum interference, we can make use of a Fano-type coupling [11] through ultrafast inelastic phonon scattering of quantum-well electrons to continuum states in the contact layer [12]. The Coulomb-scattering effect can also be included in our current many-body density-matrix equations by adding a Boltzmann-type collision integral [7]. Moreover, in this paper, we only discuss the intersubband coupling by an external electromagnetic field. For interband coupling between holes in the valence band and electrons in conduction band, an $(8\times8)-\mathbf{k}\cdot\mathbf{p}$ theory [1] must be employed for the calculation of hole states in valence band.

ACKNOWLEDGMENT

We would like to thank AHPCC, where these calculations were carried out.

[1] D.H. Huang and D. Cardimona, Phys. Rev. A **64**, 013822 (2001).
[2] P.W. Milonni, Phys. Rep. **25**, 1 (1976).
[3] D.A. Cardimona, M.G. Raymer, and C.R. Stroud, Jr., J. Phys. B **15**, 55 (1982).
[4] A. Imamoğlu and S.E. Harris, Opt. Lett. **14**, 1344 (1989).
[5] H. Fern, C. Keitel, M.O. Scully, and S.Y. Zhu, Opt. Commun. **87**, 323 (1992).
[6] D.A. Cardimona and D.H. Huang, Phys. Rev. A **65**, 033828 (2002).
[7] M. Lindberg and S.W. Koch, Phys. Rev. B **38**, 3342 (1988).
[8] D.H. Huang and M.O. Manasreh, Phys. Rev. B **54**, 5620 (1996).
[9] W.W. Chow and S.W. Koch, *Semiconductor-Laser Fundamentals—Physics of the Gain Materials* (Springer-Verlag, Berlin, 1999).
[10] G. Bastard and J.A. Brum, IEEE J. Quantum Electron. **22**, 1625 (1986).
[11] U. Fano, Phys. Rev. **124**, 1866 (1961).
[12] J. Faist, F. Capasso, C. Sirtori, A.L. Hutchinson, K.W. West, and L.N. Preiffer, Appl. Phys. Lett. **71**, 3477 (1997).